frontiers | Frontiers in Earth Science

ORIGINAL RESEARCH
published: 24 August 2022
doi: 10.3389/feart.2022.954192

Multiple-Stage Injection of Deep Hydrothermal Fluids in the Dolostone Reservoirs of Ordovician Majiagou Formation, Southern Ordos Basin

Zhaolin Yang[1,2], *Xinshe Liu*[1,2], *Xu Han*[1,2], *Hu Zhou*[1,2], *Sha Zhan*[1,2], *Xiaojun Gui*[1,2], *Jihong Niu*[1,2] *and Ke Wang*[3]*

[1]Research Institute of Exploration and Development, Changqing Oil Field Company of PetroChina, Xi'an, China, [2]National Engineering Laboratory for Exploration and Development of Low Permeability Oil and Gas Fields, Changqing Oil Field Company of PetroChina, Xi'an, China, [3]College of Geosciences and Engineering, Xi'an Shiyou University, Xi'an, China

OPEN ACCESS

Edited by:
Chen Zhang,
Chengdu University of Technology, China

Reviewed by:
Qingbin Xie,
China University of Petroleum, Beijing, China
Yannick Tepinhi,
Schlumberger (United States), United States

***Correspondence:**
Ke Wang
wangkeupc@163.com

Specialty section:
This article was submitted to Structural Geology and Tectonics, a section of the journal Frontiers in Earth Science

Received: 27 May 2022
Accepted: 15 June 2022
Published: 24 August 2022

Citation:
Yang Z, Liu X, Han X, Zhou H, Zhan S, Gui X, Niu J and Wang K (2022) Multiple-Stage Injection of Deep Hydrothermal Fluids in the Dolostone Reservoirs of Ordovician Majiagou Formation, Southern Ordos Basin. Front. Earth Sci. 10:954192. doi: 10.3389/feart.2022.954192

The Middle Ordovician Majiagou Formation in the southern Ordos Basin develops a set of sub-and peri-tidal carbonate successions that were extensively dolomitized. Diagenetic dolomitization is widely investigated because dolostones provide high-quality gas reservoirs in the southern Ordos Basin. Nonetheless, the ultimate mechanism controlling dolomitization remains enigmatic. In this study, integrated geochemical indexes including carbon and oxygen isotopes, rare earth elements, and microthermometry, coupled with U-Pb dating and lithofacies and mineralogic studies, are investigated to elucidate the periods of hydrothermal fluids involved in the formation of different types of dolomites in the studied section from Ma5 member. The results reveal that the micritic dolomite matrix was formed under the involvement of low-salinity meteoric water in the mixing zone during a shallow-burial environment. The mixing zone of paleokarst possibly provided accommodation for this dolomitization. The fine-/medium-sized dolomites were formed due to interactions between hydrothermal fluids of comparatively low temperature and matrix carbonates, which occurred during the period of the Middle Jurassic. The dolomitic microbialites were formed due to the injection of high-temperature acid fluids associated with organic matter maturing. This dolomitization occurred during the period of the Late Jurassic according to U-Pb ages. The coarse-sized dolomite cements can be furtherly classified into two types according to different U-Pb ages and carbon-oxygen isotopes, although they are very similar with respect to mineralogic features. Comprehensive geochemical evidence revealed that the dolomitizing fluids of two types of dolomite cements were derived from hydrothermal fluids associated with periodical magmatism, which occurred during the period of the Early Cretaceous. This finding provides a new insight for elucidating the diagenetic process of reservoir dolostones from the Middle Ordovician in the Ordos Basin.

Keywords: hydrothermal fluids, burial dolomitization, isotopic geochemistry, elemental geochemistry, ordos basin

1 INTRODUCTION

Compared with limestones, dolostones contribute major hydrocarbon reserves (more than 50%) in worldwide carbonate successions because the dolomitizing process usually enhances physical properties of reservoir rocks (Zenger et al., 1980; Sun, 1995; Warren, 2000; Ma et al., 2007). Multiple dolomitizing mechanisms have been proposed to explore dolomite origins, such as evaporative, seepage-reflux, microbial-mediated, and hydrothermal-fluid dolomitizations (e.g., Adams and Rhodes, 1960; Friedman and Sanders, 1967; Badiozamani, 1973; Hsu and Schneider, 1973; Baker and Kastner, 1981; Braithwaite and Rizzi, 1997; Huang et al., 2008). However, the ultimate nature of dolomites remains a subject of dispute, because it is difficult to identify precisely the origins of dolomitizing fluids due to complicated diagenetic processes and fluid-rock interactions. Hence, it is of great significance to elucidate the nature of diagenetic fluids. It is widely recognized that the interplay of diagenetic fluids and carbonate rocks exerts important controls on reservoir development in carbonate successions. The dissolution caused by different post-depositional fluids (e.g., hydrothermal fluids derived from deep-burying formation water or magmatism, organic acid, and Thermochemical sulfate reduction) can be constructive to reservoir properties (Smith, 2006; Lavoie and Chi, 2010).

The Middle Ordovician Majiagou Formation of the Ordos Basin, composed dominantly by dolostones, has been widely studied due to its abundant natural gas being reserved in karst-controlled and burial dissolution carbonate reservoirs (Dai, 2016). In previous studies, the favorable reservoir condition of the Majiagou Formation was mainly attributed to telogenetic karstification controlled by Caledonian tectonism (Chen et al., 2013; He et al., 2013). However, the dissolution process accompanying karstification was ignored. Recent studies revealed that complicated dissolving fluids occurred along fracturing systems and unconformities. For instance, high-frequency depositional cycles and subaerial exposure surfaces were identified in the Member-5 section of the Majiagou Formation (i.e., subsalt Ma5 member), implying a new type of karstification and associated later-stage fluids (Xiong et al., 2019). Moreover, hydrothermal fluids and their constructive effects on reservoir properties were identified in the Majiagou Formation (Liu et al., 2011). Nonetheless, the ultimate nature and evolution of these fluids were undocumented, which hindered our understanding of the dolomitizing process and the formation of dolostone reservoirs in this area.

Coupled with detailed hand specimens, lithofacies, petrography, and mineralogy studies, integrated isotopic/elemental geochemical proxies are analyzed in the current study to elucidate the origin and evolution of hydrothermal fluids related to reservoir formation of the Majiagou Formation, thus providing new insights for reservoir forming mechanism and prediction, as well as an analog to the occurrence of dolostone reservoirs of similar geological conditions.

2 GEOLOGICAL SETTING

The Ordos Basin, covering an area of 25×10^4 km^2, is located on the western edge of the North-China craton and consists of six tectonic structures, i.e., the Yimeng uplift, the Jinxi flexural belt, the Yishan slope, the Tianhuan depression, the western edge thrust belt, and the Weibei uplift (**Figure 1A**; Li et al., 2019). The Ordos Basin is the second largest inland basin in China, with abundant hydrocarbon resources and a thickness of more than 5,000 m of sedimentary rocks. The basement is composed of Archean and Proterozoic metamorphic rocks. The Middle-Ordovician Majiagou Formation consists of six lithologic sections (i.e., from the Ma1 to the M6 members), which represent a complete marine transgression-regression cycle upwardly (**Figure 1B**). The Majiagou Formation is a set of carbonate rocks intercalated with evaporites (He et al., 2014; Fu et al., 2017). Among them, the Ma1, the Ma3, and the Ma5 members are mainly composed of dolostones with gypsum or salty caprocks; the Ma2, the Ma4, and the Ma6 members dominantly consist of dolostones and dolomitized limestones. The gypsum and salt intercalations are mainly developed in the Ma1, the Ma3, and the Ma5 members, which indicate the depositional interval of the seawater regressive period. The Ma5 member can be furtherly divided into ten sub-members according to evaporative cycles upwardly, i.e., from Ma5-1 to Ma5-10 (**Figure 1B**). The Ma5-6 sub-member was deposited at the widest range with an area of ~50000 km^2, and the thickness of regional gypsum rocks can reach to more than 80 m, thus dividing Ordovician strata into post-salt and pre-salt period. The eighth and 10th sub-members comprise mostly gypsum/salts and gypsiferous dolomites, which were considered to deposit under a highly saline environment and act as an important source of sealing rocks (Xia et al., 2007). Intraplatform shoals and microbial mounds were intercalated developing within these sub-members, thus forming important gas reservoirs of the Ordos Basin.

3 SAMPLES AND METHODS

Cored Samples are exclusively collected from the Ma5 member in the studied area (i.e., the Fuxian area, as shown in **Figure 1A**). Specific sampling intervals are shown in **Figure 1B**. A total of 185 samples are preliminarily described and treated in the field to avoid weathering crusts or drilling mud contamination. Detailed lithofaices, petrographic, and mineralogic observations of cores and thin-sections are undertaken for subsequent isotopic and elemental analysis. A proportion of thin-sections are impregnated with epoxy resin to identify the pore system.

For stable oxygen and carbon isotopic analyses, a total of 78 powder samples (weighting 50 mg) are obtained with a dental drill of diameter 50 μm. The powder samples are subsequently reacted with HNO_3 (90% in concentration) at 72°C for 5 h linked to Finnigan Delta-V mass spectrometer. All results are recorded in per mil of V-PDB standard. The accuracy of the isotopic

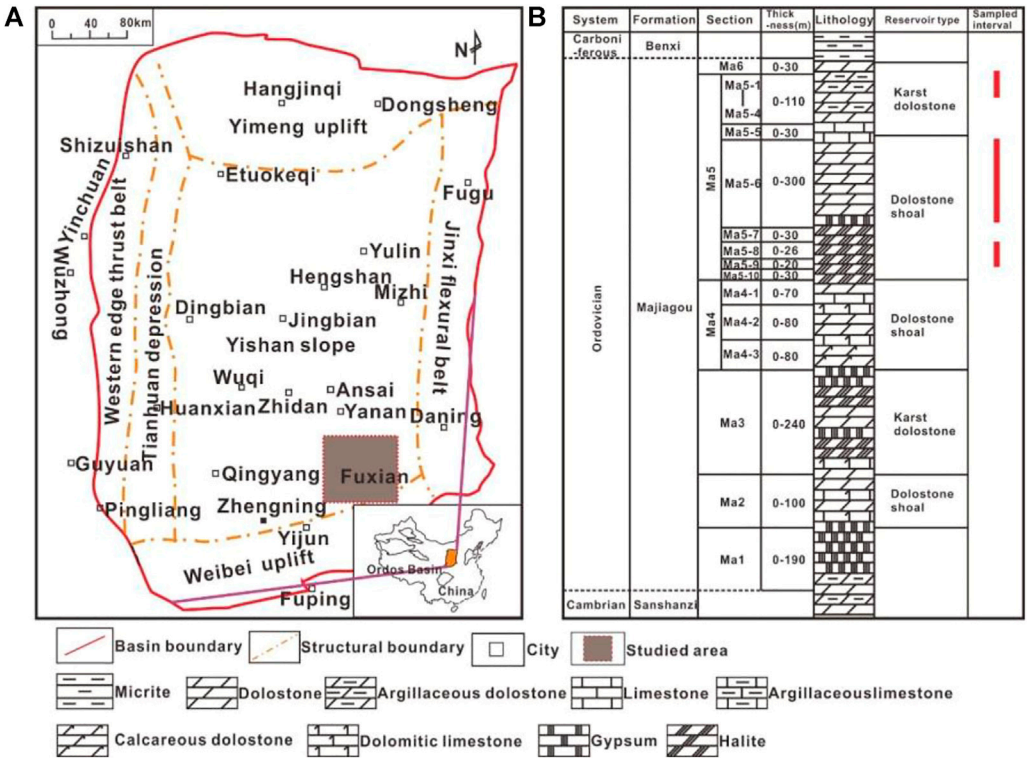

FIGURE 1 | (A) Structural units and studied location within the Ordos Basin (modified after Dai, 2016). **(B)** Lithologic column showing stratigraphy of the Majiagou Formation and sampled interval.

measurements is calibrated by replicate analyses of internal-standard NBS-19 and the analytical error is better than ±0.05‰.

For radioactive strontium isotope ($^{87}Sr/^{86}Sr$) determination, 200 mg powder dissolved in distilled water solution is prepared. The aimed samples are transferred into Teflon vials containing a mixture of 2 ml concentrated HF, 3 ml concentrated HCl and 0.5 ml HNO_3. Samples are heated at 90°C for 48 h. Subsequently, the solution is dried, redissolved in 2.0 ml HCl, and heated for 24 h $^{87}Sr/^{86}Sr$ concentrations are determined using a Neptune multi-collector ICP-MS by static measurement of ^{82}Kr, ^{83}Kr, ^{84}Sr, ^{85}Rb, ^{86}Sr, ^{87}Sr, and ^{88}Sr ion beam intensities. Corrected $^{87}Sr/^{86}Sr$ ratios are then normalized to NBS SRM 987 (certified value of 0.71024 ± 0.00025). The measurement accuracy is better than 0.00002. The detailed experimental protocol and procedure follows Boral et al. (2021).

In-situ analyses are carried out to determine trace and rare earth elements for dolomites and matrix calcites. A LSX-200 UV laser ablation system linked to Nd-YAG laser emitter and Helium carrier is applied for measurement. The diameter of the laser spot is 50 μm with a wavelength of 213 nm and an impulse frequency of 10 Hz. The detection limits range from 0.001 ppm to 1 ppm with respect to different elements, and detection precision is better than 3%. The preparation of functional thin-sections and workflows follow Liu et al. (2017).

Zircon grains from carbonate samples by magnetic and methylene iodide liquid separation. Separated zircon grains are hand-picked and fixed in epoxy resin. Subsequently, the epoxy mounts are polished for the following date measurement. The samples are dated by *in-situ* Laser Ablation Inductively-Coupled Mass Spectrometry method. The equipment is introduced above. The synthetic glass NIST-610 is applied for instrumental optimization. The standard zircon 91500 is used as an external standard. The counting time of measurement is 30 s, including the first 10 s for background measuring.

Microthermometric fluid-inclusion analyses are performed using a Linkam THMS 300 heating-freezing stage linked with an electrical microscope and microthermometric analysis software. Inclusion populations are carefully described with respect to their sizes, distribution, and vapor-liquid ratios. The micro-areas developing fluid-inclusion assemblages (FIA) are focused and then the 0.5-mm-thick thin-sections are treated with acetone solution to acquire previously focused fragments for microthermometric analysis. Homogenization temperatures (T_h) and Ice-melting temperatures (T_m) are measured on primary liquid-vapor inclusions. The detailed measurement procedure sensu Shepherd et al. (1985). Salinities were calculated in form of wt% in the H_2O-NaCl-$CaCl_2$ system using the equation proposed by Hall et al. (1988), i.e., NaCl (wt%) = $1.78T_m–0.0442T_m^2 + 0.000557T_m^3$. The measured accuracy of the T_h and T_m values are within ± 1°C and ± 0.5°C, respectively.

The above experiments were carried out at the State Key Laboratory of Petroleum Resources and Prospecting in China University of Petroleum, Beijing.

FIGURE 2 | Core sample photographs showing lithofacies of the studied interval in the Ma5 member. **(A)** Micritic dolomite matrix showing laminated layers. **(B)** Stromatolites developing thin layers of different colors. **(C)** Dolomite breccias. **(D)** Breccias collapsing in the studied interval, leaving visible fractures. **(E)** Fractures developing in bulky dolostones. **(F)** Silty dolomites developing no visible pores. **(G)** Gypsum developing in upper tidal-flat sabkha environment.

4 LITHOFACIES AND MINERALOGY

In the studied area, Silurian or Devonian strata are absent because of the uplifting of the Ordovician carbonates, thus causing longtime depositional hiatus (**Figure 1B**). Therefore, erosional surfaces of multiple levels are documented mainly at the top of deposits including intraplatform shoals, microbials, and gypsum or salt bearing strata. This typical evaporitic environment resulted in the development of micritic dolomites (**Figure 2A**). Microbialites are widely developed in the subsalt Ma5 member, mainly consisting of stromatolite. The stromatolites are characterized by regular repetition occurrence of mm-scale thin layers of different colors (**Figure 2B**). Plate-shaped and corrugated stromatolites are major types. The breccias are widely developed below the exposed surfaces with a thickness of several centimeters. The breccias exhibit dark yellowish nodular features from observed cores (**Figure 2C**), showing distinctively different contact surfaces to the surrounding dolostone matrix. Particularly, breccias collapse easily at intervals of exposed erosional surfaces (**Figure 2D**). At intervals distal from exposure surfaces, karstification did not occur widely, thus developing few breccia dolostones. Instead, dissolved pores or fractures induced by other fluids forming visible caves are observed from bulky dolostones (**Figure 2E**). Nonetheless, these pores or fractures are rarely developed in micritic dolomites, possibly due to few porosities for accommodating diagenetic fluids. These fractures are regularly distributed (**Figure 2E**), thus providing effective reservoir porosities for natural gas. Micritic-to silty-dolostones most widely occurr as matrix rocks. This type of dolostones is widely developed in the platform shoal and evaporative zone. It is featured by coarse silty to fine-sized crystals, developing no visible pores or fractures from core observation (**Figure 2F**). The gypsum and salt are generally formed by leaching and/or collapsing of upper tidal-flat sabkha environments caused by meteoric-water influx during penecontemporaneous exposure (**Figure 2G**). Carbonate silts or authigenic argillaceous infillings of grey to black colors are commonly distributed in the gypsum or salt vugs, forming a chickenwire-like structure (Zhang et al., 1991).

Various types of dolomites are developed in the studied interval of the Majiagou Formation. 1) Micritic dolomite. This type of dolomite is mainly distributed in the platform flat and associated with evaporative minerals, exhibiting anhedral to subhedral crystals with grain sizes commonly less than 20 μm (**Figure 3A**). Some scattered pyrites are variably distributed

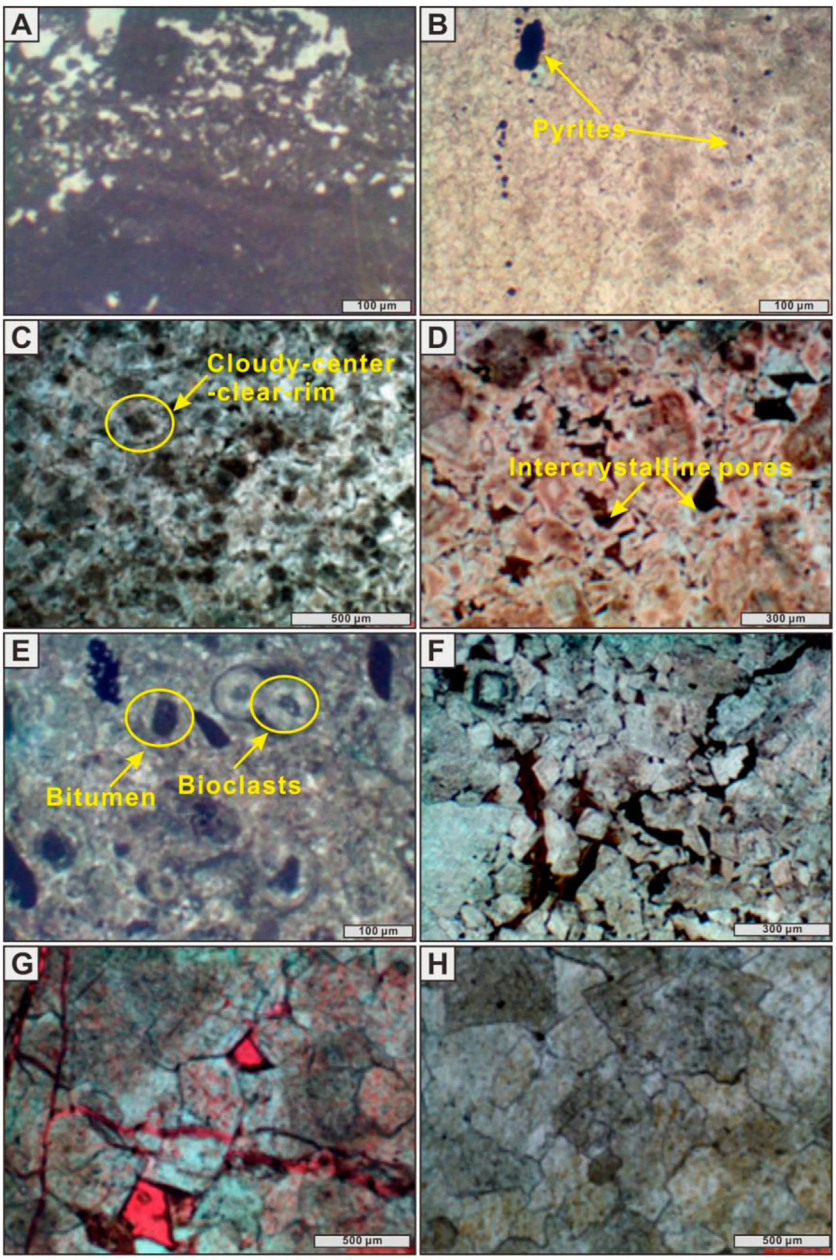

FIGURE 3 | Photomicrographs showing mineralogic features of dolostones in the studied interval under plane-polarized light. **(A)** Micritic dolomites showing anhedral to subhedral crystals with micritic grain sizes. Well-J48, 3,225.86 m. **(B)** Pyrites distributed in micritic dolomites in scatter. Well-J432, 3,584.12 m **(C)** "Cloudy-center-clear-rim" features developing medium-sized dolomite. Well-J48, 3,237.48 m. **(D)** Intercrystalline pores developing in medium-sized dolomites. Well-J48, 3,239.89 m. **(E)** Bitumen and bioclasts developing in microbialites. Well-J445, 4,105.56 m. **(F)** Residual pores are visible in medium-sized dolomites of microbialites. Well-J431, 4,425.11 m. **(G)** Dolomite cements developing intercrystalline pores. Well-J431, 4,428.91 m. **(H)** Dolomite cements composed of smaller crystals developing no porosities and exhibiting saddle shapes. Well-J52, 4,123.56 m.

within this type of dolomite, having content less than 10% in volume (**Figure 3B**). 2) Fine-to medium-sized dolomite. This type of dolomite is dominantly distributed in the middle part of meter-scale stratigraphic cycles, as well as the major construction of the carbonate matrix. Under thin-section observation, it usually displays a poikilotopic texture with euhedral to subhedral crystals and 50 μm–200 μm in crystalline sizes (**Figure 3C**). Few evaporative minerals are developed within this type of dolomite. In some coarse crystals, the texture of "cloudy-center-clear-rim" is observed (**Figure 3C**). Intercrystalline dissolved pores are widely developed with associated authigenic infillings in this type of dolomite (**Figure 3D**). 3) Dolomitic microbialites. This type of microbialites is displayed as thrombolites and stromatolites,

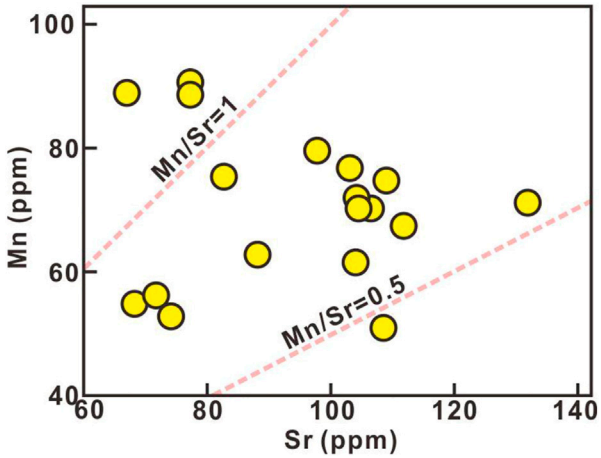

FIGURE 4 | Crossplot showing Mn/Sr ratios of the micritic dolomites.

both containing biotic debris and reflecting a high-energy shallow-water environment (**Figure 3E**). The microibalites usually exhibit cluster and granular structures and grid textures. Only a small proportion of residual pores are visible due to agglutinates filling (**Figure 3F**). Bituminous fillings are commonly developed in dolomitic microbialites (**Figure 3E**). 4) Dolomite cements. The dolomite cements consist of coarse crystals with sizes ranging from 400 μm to 1,000 μm, which generally occur as authigenic minerals filling in dissolved vuggy pores in the matrix dolostones. This type of dolomites exhibits planar euhedral to subhedral. The large-sized dolomites commonly develop intercrystalline porosities (**Figure 3G**). By contrast, the dolomite cements of comparatively smaller crystals usually develop no porosities (**Figure 3H**). Meanwhile, some authigenic minerals such as quartz and fluorite are associated with large-sized dolomite cements (i.e., saddle dolomite).

5 RESULTS AND DISCUSSION

5.1 Dolomitization of Matrix Dolomites

In the eastern Ordos Basin, the occurrence of widespread micritic dolostones has been previously interpreted as the product of seepage-reflux dolomitization (Yang et al., 2018). However, its ultimate mechanism in the studied area is remaining unsolved. The Sr concentrations decrease with increasing burial depth during dolomitization (Liu et al., 2016). The micritic dolomite matrix exhibits Sr values ranging from 77 ppm to 135 ppm (mean value of 92 ppm), which is consistent with Sr content in normal seawater (i.e., less than 550 ppm; Tucker and Wright, 1990). Meanwhile, the Mn content of the matrix dolomite ranges from 55 ppm to 86 ppm with a mean value of 68 ppm, reflecting little influence on diagenesis because the Mn/Sr ratios are exclusively less than 2 (**Figure 4**; Huang et al., 2008). However, the $\delta^{13}C$ values are slightly negative and out of the range of seawater origin (**Figure 5**), suggesting that this type of dolomite may not be formed in a typical marine environment. Diagenesis with meteoric water involvement should result in dolomites characterized by negative $\delta^{13}C$ composition (Swart et al., 2005). Meanwhile, the $\delta^{18}O$ values of the matrix dolomite (mean value of −8.05‰, V-PDB) are more pronouncedly depleted than the published ratios for Ordovician seawater (i.e., −6.6‰ to −4.0‰; Allen and Wiggins, 1993). This result indicates that the micritic dolomite matrix was formed under the involvement of meteoric fluids. This is also consistent with the distribution pattern of the rare earth elements of the micritic dolomites, which are different from seawater-origin micritic limestones (**Figure 6A**). The calculated salinity of this type of dolomite is Z = 105.5 using equation proposed by (Keith and Weber 1964) [i.e., Z = 2.048 ($\delta^{13}C_{PDB}$ + 50) + 0.498 ($\delta^{18}O_{PDB}$ + 50)].

Presumably, the matrix dolomites were formed under a low-salinity environment with the involvement of meteoric water at the mixing zone during the shallow-burial stage. The mixing zone possibly provided accommodation for widespread dolomitization. It is noteworthy that this dolomitization occurred at a normal burial

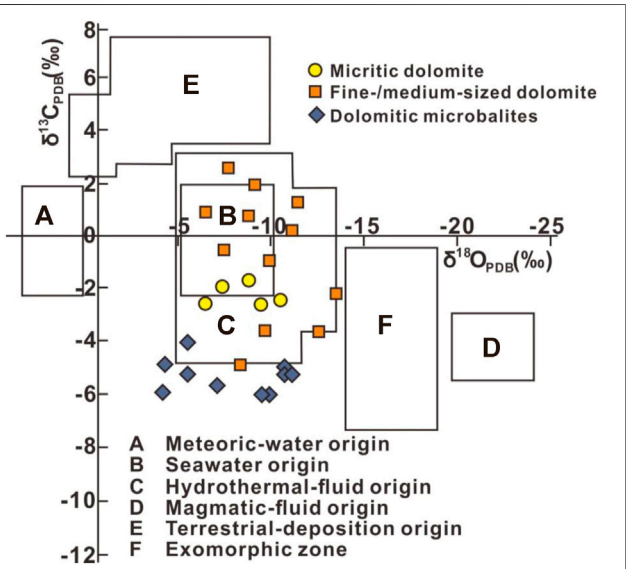

FIGURE 5 | Crossplot showing carbon and oxygen isotope features of different types of dolomites. The isotopic ranges are referred from Li et al. (2011).

temperature, as is evidenced by the homogenization temperature (i.e., mean value of 85°C; **Figure 7A**).

5.2 Multi-Stage of Hydrothermal Dolomitizing Fluids

To determine the absolute ages of crystalline dolomites (i.e., crystal sizes larger than 50 μm), U-Pb dating has been conducted for quantitative measurement. The result shows that different dolomites were formed at different diagenetic stages. The recrystallized fine-to medium-sized dolomites were formed at the earliest geological period, with measured U-Pb age of 494 ± 12 Ma and 498 ± 36 Ma, respectively (**Figures**

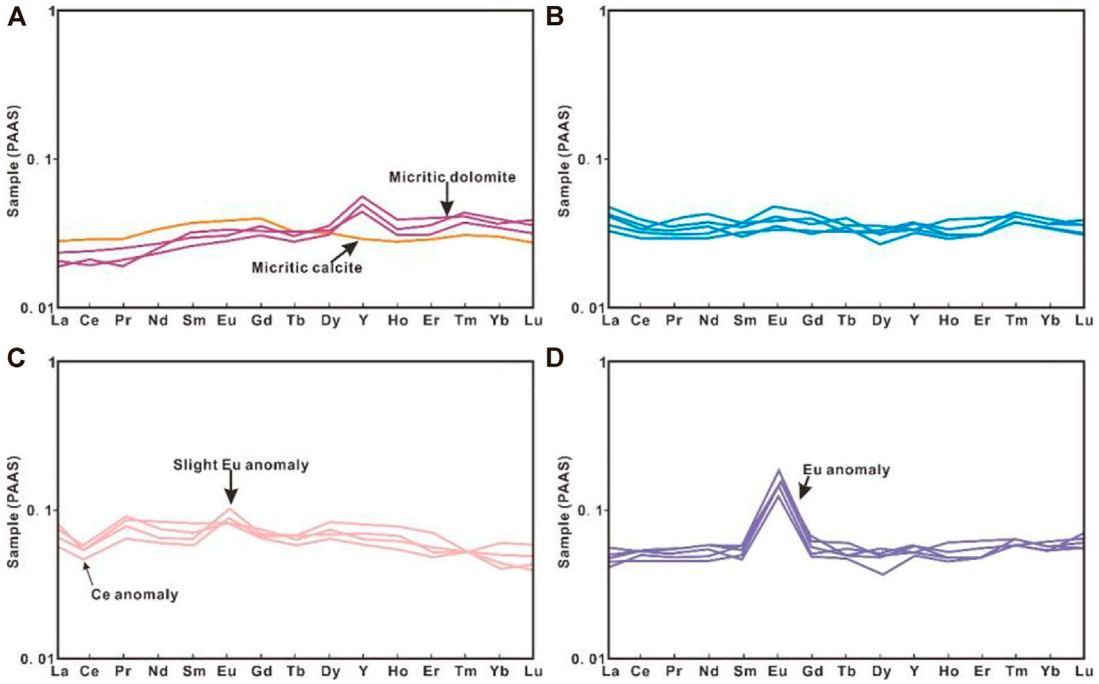

FIGURE 6 | Distribution patterns of the rare earth elements in different types of dolomites or calcites. **(A)** Micritic dolomites and calcites. **(B)** Fine-to medium-sized dolomites. **(C)** Medium-to coarse-sized dolomites. **(D)** Dolomite cements. All samples are normalized to PAAS standard (Gromet et al., 1985).

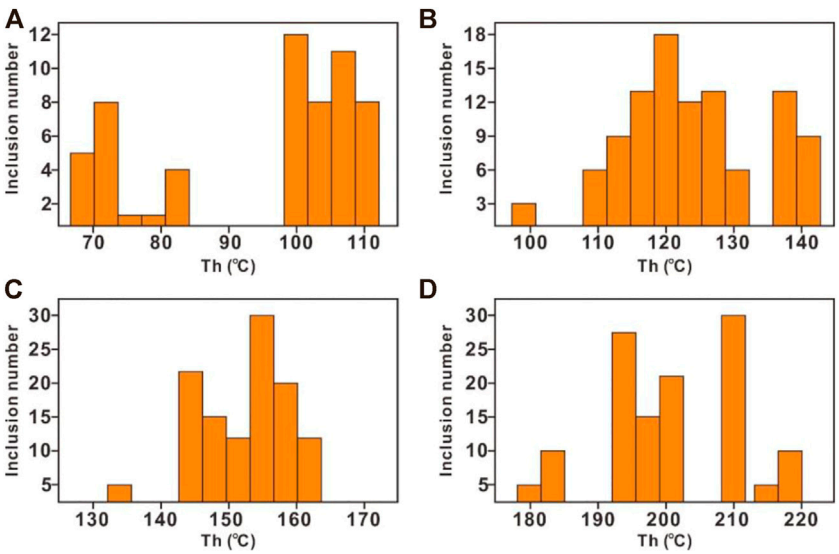

FIGURE 7 | Histograms showing homogenization temperatures of different types of dolomites. **(A)** Micritic dolomite matrix. **(B)** Fine-to medium-sized dolomites. **(C)** Medium-to coarse-sized dolomites. **(D)** Dolomite cements.

8A,B), which is equivalent to Middle Jurassic. The dolomitic microbialites were formed at a later-stage after burial, with measured U-Pb age ranging from 474 ± 31 Ma to 480 ± 12 Ma (**Figures 8C–E**). It is equivalent to Late Jurassic. The dolomite cements of large-sized crystals were formed at the latest stage, which can be further classified into two periods, i.e., 459 ± 6 Ma –466 ± 11 Ma and 440 ± 15 Ma –445 ± 11 Ma (**Figures 8F–I**). This period of geological time is equivalent to the Early Cretaceous.

For pervasively distributed fine-/medium-sized dolomites, the calculated homogenization temperatures range from 96°C to 143°C, with a mean value of 126°C (**Figure 7B**), which is

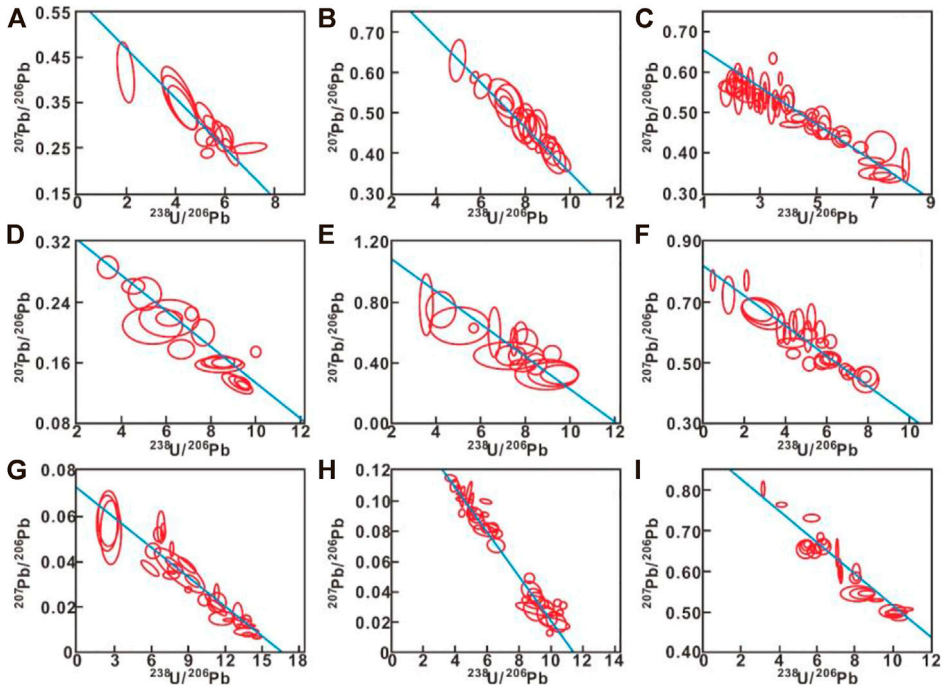

FIGURE 8 | U-Pb ages from carbonate minerals using LA-ICP-MS method. **(A)** Fine-sized dolomite, age of 494 ± 12 Ma. **(B)** Fine-sized dolomite, age of 498 ± 36 Ma. **(C)** Dolomitic microbialite, age of 474 ± 31 Ma. **(D)** Dolomitic microbialite, age of 480 ± 12 Ma. **(E)** Dolomitic microbialite, age of 477 ± 12 Ma. **(F)** Dolomite cement, age of 466 ± 11 Ma. **(G)** Dolomite cement, age of 459 ± 6 Ma. **(H)** Dolomite cement, age of 440 ± 15 Ma. **(I)** Dolomite cement, age of 445 ± 11 Ma.

approximately 10°C higher than burial temperature during the Middle Jurassic (i.e., 125°C according to the thermal gradient of 2.5°C and burial depth of 2,800 m; Lei et al., 2020). Moreover, the carbon and oxygen isotopes are plotted at the zone of "hydrothermal-fluid origin" (**Figure 5**), indicating that this type of dolomitizing fluid was featured by a hydrothermal source. Nonetheless, the distribution pattern of REEs shows seawater-like composition, but has no positive Eu anomaly (**Figure 6B**). Presumably, this type of dolomites was formed due to interactions between hydrothermal fluids of comparatively low temperature and matrix carbonates (Liu et al., 2017).

For medium-to large-sized dolomites composing microbialites, the introduction of organic matter provided probable dolomitizing fluids, because bituminous matters are widely developed within microbialites (**Figure 3E**). This inference is supported by other geochemical proxies. Firstly, this type of dolomites shows much depleted carbon isotopes with $\delta^{13}C$ values ranging from −4.05‰ to −6.18‰ and a mean value of −5.33‰ (**Figure 5**). These depleted carbon isotopes may result from the interplay of organic matter featured by extremely low $\delta^{13}C$ composition and normal marine carbonates (e.g., Meyer et al., 2011). Secondly, this type of dolomites displays REE distribution pattern that is distinctively different from marine origin carbonates (**Figure 6C**). Particularly, negative Ce anomalies (i.e., δCe mean values of 0.75; **Figure 6C**)

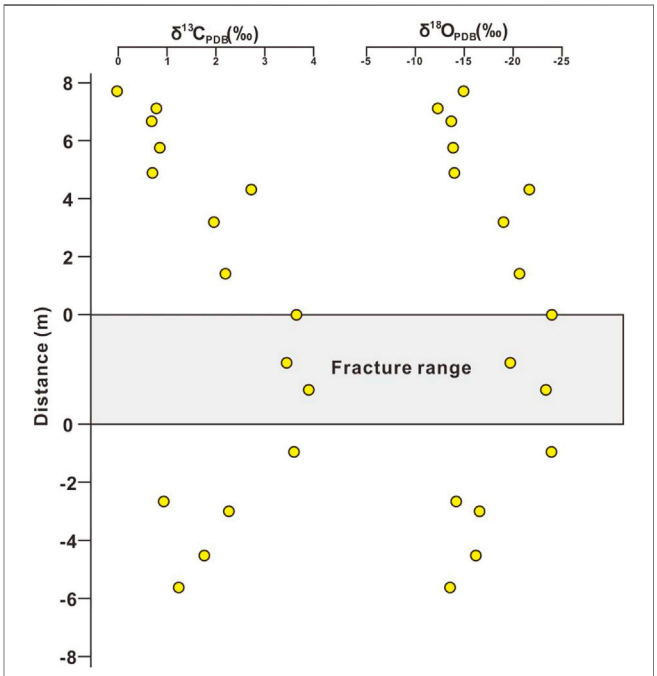

FIGURE 9 | Evolution of carbon and oxygen isotopes of dolomite cements at different ranges from fractures.

indicate a reduced environment, which is consistent with the environment for preservation of organic matter. Moreover, the microthermometric data reveals that the homogenization temperatures range from 134°C to 163°C with a mean value of 157°C (**Figure 7C**), which is consistent with a slight Eu anomaly (i.e., δEu mean value of 1.35; **Figure 6C**). To conclude, it is probably that the injection of high-temperature acid fluids associated with organic matter maturing has caused dolomitization and related dissolution.

Coarse-sized dolomite cements exhibit similar petrologic (**Figures 3G,H**) and REE distribution patterns (**Figure 6D**) although having different U-Pb ages. This may indicate that two types of dolomite cements were derived from similar origins but temporally discontinued. The microthermometric data reveals that two stages of homogenization temperature exist, i.e., the mean values of −195°C and −215°C, respectively (**Figure 7D**), which are significantly higher than temporal burial temperature. This indicates that the dolomitizing fluids are characterized by super-high temperatures, which is verified by pronouncedly positive Eu anomaly of dolomite cements (i.e., δEu mean value of 1.70; **Figure 6D**). To determine the ultimate differences of two type of hydrothermal fluids, the evolution patterns of $\delta^{13}C$ and $\delta^{18}O$ values are analyzed according to different distances from fractures. The result shows that the dolomite cements filling in major fractures display high $\delta^{13}C$ value and low $\delta^{18}O$ value (mean value of 3.3‰ and −23.5‰, respectively). On the contrary, the $\delta^{13}C$ and $\delta^{18}O$ values from dolomite cements decrease or increase linearly with increasing distances from visible fractures (**Figure 9**). This reflects that the dolomitizing fluids of two stages were derived from hydrothermal fluids associated with periodical magmatism because all previous proxies are consistent with features of magmatic fluids. Moreover, this inference is also evidenced by periodical volcanism occurring in the Ordos Basin (Li and Gao, 2010; Lei et al., 2020).

6 CONCLUSION

According to the current study, the following conclusions can be drawn:

(1) The recrystallized fine- and medium-sized dolomites were formed in the geological period equivalent to Middle Jurassic. The dolomitic microbialites were formed at a later stage after burial. This stage is equivalent to Late Jurassic. The dolomite cements of large-sized crystals were formed at the latest stage, which can be further classified into two periods (i.e., 459 ± 6 Ma −466 ± 11 Ma and 440 ± 15 Ma −445 ± 11 Ma). This period of geological time is equivalent to the Early Cretaceous.
(2) The matrix dolomites were formed under a low-salinity environment with the involvement of meteoric water at the mixing zone during the shallow-burial stage. The mixing zone possibly provided accommodation for the occurrence of dolomitization.
(3) The fine-to medium-sized dolomites were formed because of the interplay between hydrothermal fluids of comparatively low temperature and matrix carbonates.
(4) The medium-to large-sized dolomites were formed because of injection of high-temperature acid fluids associated with organic matter maturing, which has caused dolomitization and related dissolution.
(5) The two types of dolomite cements were derived from similar origins but temporally discontinued. The geochemical proxies reveal that dolomitizing fluids of two stages were derived from hydrothermal fluids associated with periodical magmatism.

DATA AVAILABILITY STATEMENT

The original contributions presented in the study are included in the article/Supplementary Material, further inquiries can be directed to the corresponding author.

AUTHOR CONTRIBUTIONS

ZY: conceptualization, methodology, writing—review and editing. XL: formal analysis, investigation, visualization. XH: formal analysis, investigation, visualization. HZ: formal analysis, investigation, visualization. SZ: formal analysis, investigation, visualization. XG: formal analysis, investigation, visualization. JN: formal analysis, investigation. KW: methodology, project administration.

ACKNOWLEDGMENTS

The reviewers are thanked for their valuable comments.

REFERENCES

Adams, J. E., and Rhodes, M. L. (1960). Dolomitization by seepage refluxion. *AAPG Bull.* 44 (12), 1912–1920. doi:10.1306/0BDA6263-16BD-11D7-8645000102C1865D

Allen, J. R., and Wiggins, W. D. (1993). Dolomite reservoirs: Geochemical techniques for evaluating origin and distribution. *J. Pet. Sci. Eng.* 14, 262–263. doi:10.1306/CE36576

Badiozamani, K. (1973). The dorag dolomitization modeldapplication to the middle Ordovician of Wisconsin. *J. Sediment. Pet.* 43 (4), 965–984.

Baker, P. A., and Kastner, M. (1981). Constraints on the formation of sedimentary dolomite. *Science* 213 (4504), 214–216. doi:10.1126/science.213.4504.214

Boral, S., Peucker-Ehrenbrink, B., Hemingway, J. D., Sen, I. S., Galy, V., and Fiske, G. J. (2021). Controls on short-term dissolved 87Sr/86Sr variations in large rivers: Evidence from the Ganga–Brahmaputra. *Earth Planet. Sci. Lett.* 566, 116958–117012. doi:10.1016/j.epsl.2021.116958

Braithwaite, C. J. R., and Rizzi, G. (1997). The geometry and petrogenesis of hydrothermal dolomites at Navan, Ireland. *Sedimentology* 443, 421–440. doi:10.1046/j.1365-3091.1997.d01-30.x

Chen, H. D., Hu, S. H., Chen, A. Q., Zhao, J. X., and Su, Z. T. (2013). Genesis of non-karst dolomite reservoirs in the eastern central paleo-uplift in the Ordos Basin. *Nat. Gas. Ind.* 33, 18–24. (in Chinese with English abstract). doi:10.3787/j.issn.1000-0976.2013.10.003

Dai, J. X. (2016). *Giant coal-derived gas fields and their gas sources in China*. Beijing: Science Press, 1–564.

Friedman, I., and Sanders, J. E. (1967). "Origin and occurrence of dolostone," in *Carbonate rocks*. Editors G. V. Chilingar, H. J. Bissel, and R. W. Fairbridge (Amsterdam: Elsevier), 267–348.

Fu, J. H., Wu, X. N., Sun, L. Y., Yu, Z., Huang, Z. L., and Ding, Z. C. (2017). New understandings of the lithofacies paleogeography of the middle assemblage of Majiagou Fm in the Ordos Basin and its exploration significance. *Nat. Gas. Ind. B* B4 (4), 278–286. doi:10.1016/j.ngib.2017.08.011

Gromet, L. P., Haskin, L. A., Korotev, R. L., and Dymek, R. F. (1985). The "north aAmericanshale composite": Its compilation, major and trace element characteristics. *Geochim. Cosmochim. Acta* 48 (12), 2469–2482. doi:10.1016/0016-7037(84)90298-9

Hall, D. L., Sterner, S. M., and Bodnar, R. J. (1988). Freezing point depression of NaCl-KClH2O solutions. *Econ. Geol.* 83, 197–202. doi:10.2113/gsecongeo.83.1.197

He, J., Fang, S. X., Hou, F. H., Yan, R. H., Zhao, Z. J., Yao, J., et al. (2013). Vertical zonation of weathered crust ancient karst and the reservoir evaluation and prediction—A case study of M55–M51 sub-members of Majiagou Formation in gas fields, central Ordos Basin, NW China. *Pet. explor. Dev.* 40, 534–542.

He, X. Y., Shou, J. F., Shen, A. J., Wu, X. N., Wang, Y. S., Hu, Y. Y., et al. (2014). Geochemical characteristics and origin of dolomite: A case study from the middle assemblage of ordovician Majiagou Formation member 5 of the west of jingbian gas field, Ordos Basin, north China. *Petroleum Explor. Dev.* 41 (3), 417–427. doi:10.1016/s1876-3804(14)60048-3

Hsu, K. J., and Schneider, J. (1973). *Progress report on dolomitization hydrology of AbuDhabi sabkhas, arabian gulf. The Persian gulf*. New York: Springer, 409–422.

Huang, S., Qing, H., Huang, P., Hu, Z., Wang, Q., Zou, M., et al. (2008). Evolution of strontium isotopic composition of seawater from Late Permian to Early Triassic based on study of marine carbonates, Zhongliang Mountain, Chongqing, China. *Sci. China Ser. D-Earth. Sci.* 51 (4), 528–539. doi:10.1007/s11430-008-0034-3

Keith, M. L., and Webber, J. N. (1964). Carbon and oxygen isotopic composition of selected limestones and fossils. *Geochim. Cosmochim. Acta* 28, 1787–1816. doi:10.1016/0016-7037(64)90022-5

Lavoie, D., and Chi, G. X. (2010). Lower Paleozoic foreland basins in eastern Canada: Tectono-thermal events recorded by faults, fluids and hydrothermal dolomites. *Bull. Can. Petroleum Geol.* 58 (1), 17–35. doi:10.2113/gscpgbull.58.1.17

Lei, H., Huang, W., Yi, S., and Wang, Y. (2020). Dissolution characteristics of deep-buried dolostone in the member 5 of ordovician Majiagou Formation in southern Ordos Basin. *J. Palaeogeograh. Chin. Ed.* 22 (6), 1041–1052.

Li, M., and Gao, J. R. (2010). Basement faults and volcanic rock distributions in the Ordos Basin. *Sci. China Earth Sci.* 40 (8), 1005–1013.

Li, P., Ren, J., Yang, H., Hu, D., and Zhang, Y. (2011). Hydrothermal activities in the fault system and their effects on carbonate rocks in the Bachu Area. *Geotect. Metallogenia* 35 (3), 378–385. doi:10.1016/j.marpetgeo.2020.104506

Li, Y., Gao, X., Meng, S., Wu, P., Niu, X., Qiao, P., et al. (2019). Diagenetic sequences of continuously deposited tight sandstones in various environments: A case study from upper paleozoic sandstones in the linxing area, eastern Ordos Basin, China. *Am. Assoc. Pet. Geol. Bull.* 103, 2757–2783. doi:10.1306/03061918062

Liu, C., Xie, Q., Wang, G., He, W., Song, Y., Tang, Y., et al. (2017). Rare Earth element characteristics of the carboniferous huanglong formation dolomites in eastern sichuan basin, southwest China: Implications for origins of dolomitizing and diagenetic fluids. *Mar. Pet. Geol.* 81, 33–49. doi:10.1016/j.marpetgeo.2016.12.030

Liu, C., Xie, Q., Wang, G., Song, Y., and Qi, K. (2016). Dolomite origin and its implication for porosity development of the carbonate gas reservoirs in the Upper Permian Changxing Formation of the eastern Sichuan Basin, Southwest China. *J. Nat. Gas. Sci. Eng.* 35, 775–797. doi:10.1016/j.jngse.2016.09.027

Liu, Y., Fu, J. H., and Li, J. M. (2011). Dolomite genetic analysis on ordovician Majiagou Formation in eastern Ordos Basin. *J. Oil Gas. Technol.* 33 (11), 46–50.

Ma, Y., Guo, X., Guo, T., Huang, R., Cai, X., and Li, G. (2007). The puguang gas field: New giant discovery in the mature sichuan basin, southwest China. *Am. Assoc. Pet. Geol. Bull.* 91 (5), 627–643. doi:10.1306/11030606062

Meyer, K. M., Yu, M., Jost, A. B., Kelley, B. M., and Payne, J. L. (2011). δ13C evidence that high primary productivity delayed recovery from end-Permian mass extinction. *Earth Planet. Sci. Lett.* 302, 378–384. doi:10.1016/j.epsl.2010.12.033

Shepherd, T. J., Rankin, A. H., and Alderton, D. H. M. (1985). *A practical guide to fluid inclusion studies*. London: Blackie.

Smith, L. B., Jr. (2006). Origin and reservoir characteristics of Upper Ordovician Trenton-Black River hydrothermal dolomite reservoirs in New YorkRiver hydrothermal dolomite reservoirs in New York. *Am. Assoc. Pet. Geol. Bull.* 90 (11), 16911718–1718. doi:10.1306/04260605078

Sun, S. Q. (1995). Dolomite reservoirs: Porosity evolution and reservoir characteristics. *AAPG Bull.* 79 (2), 186–204. doi:10.1306/8D2B14EE-171E-11D7-8645000102C1865D

Swart, P. K., Eberli, G. P., and Katz, D. (2005). The nature of the δ13C of periplatform sediments: Implications for stratigraphy and the global carbon cycle. *Sediment. Geol.* 175, 115–129. doi:10.1016/j.sedgeo.2004.12.029

Tucker, M. E., and Wright, V. P. (1990). *Carbonate sedimentology*. Oxford: Blackwell Scientific Publications.

Warren, J. (2000). Dolomite: Occurrence, evolution and economically important associations. *Earth. Sci. Rev.* 52 (1), 1–81. doi:10.1016/s0012-8252(00)00022-2

Xia, M. J., Zhen, C. B., Dai, J. X., Zhou, C. N., Wang, Z. C., and Wang, L. P. (2007). Ordovician under-salt reservoirs and forming conditions of gas poolsin in eastern Ordos Basin. *Nat. Gas. Geosci.* 18, 204–208. (in Chinese with English abstract). doi:10.1177/0144598718778171

Xiong, Y., Tan, X., Zuo, Z., Zou, G., Liu, M., Liu, Y., et al. (2019). Middle Ordovician multi-stage penecontemporaneous karstification in North China: Implications for reservoir Genesis and sea level fluctuations. *J. Asian Earth Sci.* 183, 103969–104014. doi:10.1016/j.jseaes.2019.103969

Yang, X. Y., Mei, Q. Y., Wang, X. Z., Dong, Z. X., Li, Y., and Huo, F. (2018). Indication of rare Earth element characteristics to dolomite petrogenesis-a case study of the fifth member of Ordovician Majiagou Formation in the Ordos Basin, central China. *Mar. Pet. Geol.* 92, 1028–1040. doi:10.1016/j.marpetgeo.2017.12.004

Zenger, D. H., Dunham, J. B., and Ethington, R. L. (1980). Concepts and models of dolomitization. *SEPM Spec. Publ.* 28, 1–320. doi:10.2110/pec.80.28

Zhang, J. S., Zeng, S. H., Huang, J. S., and Ma, Z. F. (1991). The occurrence and Significance of halite in eastern Ordos. *Acta Sedimentol. Sin.* 9, 34–43. (in Chinese with English abstract).

Conflict of Interest: The authors declare that the research was conducted in the absence of any commercial or financial relationships that could be construed as a potential conflict of interest.

Publisher's Note: All claims expressed in this article are solely those of the authors and do not necessarily represent those of their affiliated organizations, or those of the publisher, the editors and the reviewers. Any product that may be evaluated in this article, or claim that may be made by its manufacturer, is not guaranteed or endorsed by the publisher.